A Hybrid Cable-Driven Actuation System for Exosuits Exploiting Multistable Elastic Shells: Design and Preliminary Validation

Camilla Baselli[1], Marco Lupi[1], Jacopo Quaglierini[1],
Sophie Skach[1], Yuan Zhou[1], Leonardo Cappello[1], *Senior Member*

***Abstract*— Wearable robotics have long been proposed as a solution to augment or restore hand function, which is critical for daily autonomy. Soft robotic gloves represent a promising approach, as they can operate in parallel with human muscles while ensuring comfort and compliance. Although cable-driven designs are among the most widely adopted soft actuation solutions, they are often hindered by inefficiencies brought by friction, backlash, and the requirement for continuous motor engagement to maintain static postures, resulting in increased power consumption and reduced battery life. This work presents a hybrid actuation paradigm, which integrates nonlinear multistable elastic shells with a cable-driven transmission to empower hand exosuits. By leveraging the stable equilibrium states of the shells, the cable-driven system is used primarily to trigger snap-through transitions between straight and curled configurations, thus functionally decoupling static posture maintenance from active motor control. Bench tests on a mock-up finger demonstrate that triggering transitions between stable equilibrium states enables posture holding with near-zero motor power consumption and fast finger closure time of 0.53±0.13 s across repeated snap-through events, with motion primarily governed by shell dynamics. These findings suggest that multistable elastic elements can enhance both responsiveness and efficiency of hand exosuits, potentially contributing to the design of more and more portable and energy-efficient assistive technologies.**

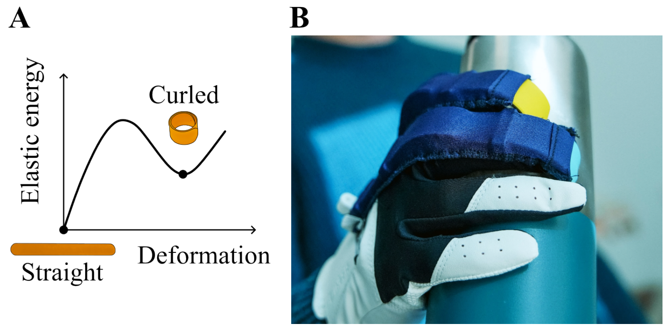

Fig. 1: (**A**) Slap-bracelets change equilibrium configuration with small energy inputs (e.g., via a tip torque). (**B**) Picture of an early prototype hand exosuit using the snap-through mechanism of multistable shells.

I. INTRODUCTION

Since their inception in the late 1960s [1], robotic exoskeletons have aimed at augmenting or restoring motor function by fusing human motion intention with robotic actuation. Since then, exoskeletons have evolved into fully wearable systems, capable of supporting limb movement and reducing physical stress in both clinical rehabilitation and industrial settings, particularly for hand assistance [2],[3]. Despite modern exoskeletons are way sleeker, lighter and more ergonomic than the rigid exoskeletons [1], they still face similar limitations to their translation to the market, hampering their widespread adoption. These architectures can deliver high and precisely controlled forces, but they are characterized by non-negligible bulk and weight. These issues are further deepened by the anatomical complexity of the human hand, where poor alignment result in reduced comfort, limited adaptability, and constrained usability during prolonged or everyday tasks.

To address these challenges, soft robotic exoskeletons have emerged as a promising alternative solution, prioritizing comfort, compliance, and wearability by leveraging flexible materials and distributed actuation. This is particularly useful when it comes to dexterous tasks in hand exosuits. However, current soft actuation strategies present significant trade-offs that limit their effectiveness. Among them, cable-driven exosuits, made from lightweight materials, have gained popularity due to their comfortable and adaptable nature [4], and possibly represent the most technologically ready solution for a wide implementation [5]. Although promising, cable-driven actuation typically suffer from friction and backlash, thus reduced efficiency, control accuracy, and speed under dynamic loads [6]. Continuous actuator engagement to maintain static postures also increases power consumption, limiting battery life and autonomy [7].

To overcome the limitations of current systems in terms of energy consumption and response-time, we propose the integration of nonlinear multistable elastic shells with cable-driven actuation. These shells, exemplified by a carpenter's measuring tape or a slap bracelet (Figure 1A), are characterized by multiple equilibrium states at different energy levels, between which they can snap with a minimal energy input [8], [9]. The main concept is to use cable-driven actuation exclusively to trigger the state changes in the multistable shells, from "straight" to "curled" configurations and vice versa, and to control the transition speed. In principle, by relying on the equilibrium states of the shells, with this

*The work of L.C. was co-funded by the European Union (ERC, MUSE, G.A. 101116249). Views and opinions expressed are however those of the author(s) only and do not necessarily reflect those of the European Union or the European Research Council. Neither the European Union nor the granting authority can be held responsible for them.

[1]All authors are with The BioRobotics Institute and the Department of Excellence in Robotics and AI, Scuola Superiore Sant'Anna Pisa, Italy. camilla.baselli@santannapisa.it, leonardo.cappello@santannapisa.it

approach we could decouple static posture holding from active motor control, with a potential significant decrease in energy consumption [10]. To investigate the applicability of this approach to hand assistance, we developed an actuation unit where two multistable shells are driven by a cable system and positioned on the dorsal side of the finger. Shells and cables are interfaced through a distal triggering mechanism based on a rigid tip lever, to minimize the cable tension required for shell activation. Our ultimate goal is to integrate these individual actuation units onto a support glove to devise a hybrid hand-assistive device: state transitions of multistable shells would enable fast, passive hand closure with minimal energy input, thereby increasing actuation bandwidth while reducing the power drawn by the motors. In this study, system performance is evaluated on a single actuation unit mounted on a mock-up finger, investigating two main aspects: energy efficiency and dynamic behavior. Specifically, triggering cable tension thresholds were measured across six alternative tip lever designs to identify the configuration minimizing both activation force and geometric footprint, and electrical power consumption was evaluated to confirm our hypothesis on energy-free posture maintenance. We assessed actuation speed and controllability through bandwidth analysis and dynamic measurements during snap-through transitions.

II. BACKGROUND

A. Multistable Shell Mechanics

The shells are modeled as isotropic, prestressed curved cylindrical strips [11]. These structures are commonly approximated as thin plates under the assumption of a small thickness-to-length ratio ($t/L \ll 1$) [11], [12], [8] and are described within the framework of classical thin-plate lamination theory [13]. The constitutive relationship between the generalized stress vector $[N_x, N_y, N_{xy}, M_x, M_y, M_{xy}]^T$ and the generalized strain vector $\Delta[\varepsilon_x, \varepsilon_y, \gamma_{xy}, k_x, k_y, k_{xy}]^T$ is expressed through the ABD matrix formulation,

$$\begin{bmatrix} N \\ M \end{bmatrix} = \begin{bmatrix} A & B \\ B & D \end{bmatrix} \Delta \begin{bmatrix} \varepsilon \\ k \end{bmatrix},$$

where **N** represents the in-plane membrane forces per unit length, **M** represents the bending and twisting moments per unit length, **A** is the extensional stiffness matrix, **B** is the bending–stretching coupling matrix, and **D** is the bending stiffness matrix. The generalized strain vectors are defined as $k = [k_x, k_y, k_{xy}]^T$ and $\varepsilon = [\varepsilon_x, \varepsilon_y, \gamma_{xy}]^T$, representing curvature and membrane strain variations with respect to the reference configuration, respectively. The mechanical behavior of multistable shells is governed by the elastic potential energy accumulated during deformation. Prestresses introduced during the manufacturing process generate internal bending stresses that are balanced by membrane stresses. As a result, the total potential energy (U_t) is defined as the sum of the bending energy (U_b) and the prestress energy (U_p),

$$U_t = U_b + U_p .$$

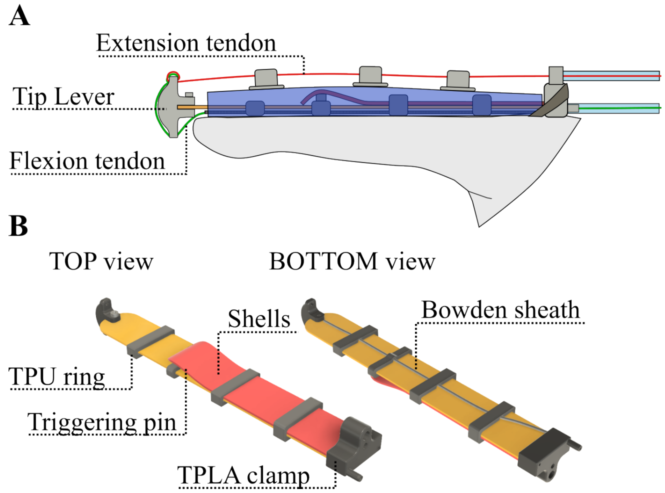

Fig. 2: **(A)** Sketch of a finger equipped with the actuation unit. Multistable shells are inserted into a pocket on the dorsal side of a support glove. Both flexion and extension cables are knotted to the triggering tip lever. (**B**) Top and bottom views of the multistable shells.

The resulting energy landscape exhibits two local minima, which define the actuation threshold, namely the minimum energy that the tendon-driven system must provide to trigger the snap-through transition between stable configurations.

III. DESIGN AND INTEGRATION

The design focuses on the physical integration of the cables with the shells to ensure reliable triggering and efficient power transmission. A single actuation unit, shown in Figure 2A, is composed of:

- *Multistable Shells*
- *Cable Routing*
- *Triggering Tip Lever*

The actuation unit integrates two overlaid shells acting in parallel (Figure 2B): a longer bottom shell, which terminates with a rounded tip at the distal phalanx, and a shorter top shell that extends slightly beyond the Metacarpophalangeal joint (MCP). Based on our preliminary observations, this configuration improves actuation performance by increasing stiffness at the MCP and enabling rapid snap-through, while keeping the system simple and lightweight, since the complete actuation unit weighs approximately 30 g.

The actuation unit is designed to be then integrated in a dedicated pocket onto a custom glove via a modular assembly process, allowing quick insertion and removal for maintenance or reconfiguration. The system is driven by two identical remote cable-driven actuation modules, respectively dedicated to flexion and extension.

A. Multistable Shells

The multistable shells have been sourced from commercially available snap bracelets (215 x 20 mm), cut to match the mock-up of an index finger dimensioned on the 50th male percentile [14]. A custom 3D-printed tPLA clamp anchors the proximal ends of both shells near the metacarpal region, immediately before the MCP. This ensures proper alignment with finger kinematics, retaining the proximal extremities of the shells in a straight configuration also during flexion, and facilitates triggering to straight configuration during extension. The two shells are fastened together by flexible TPU rings placed around them, which couple their motion while preserving multistable behavior. One of these rings, mounted on the bottom shell, features a rounded triggering pin that presses against the distal end of the top one: due to this feature, the top shell is kept in a partially bent state, while its complete snapping is prevented by the presence of the bottom one.

B. Cable Routing

The routing system is designed to provide antagonistic control of the shell's states, driving flexion and extension.

- *Flexion Routing*: The flexion cable runs through a Bowden sheath (⌀1 mm) along the underside of the bottom shell. It is guided by the flexible TPU rings, that maintain it adherent and aligned with the shells during curvature changes. The distal end of the cable is passed through the bottom hole of the triggering tip lever and knotted to the top part.
- *Extension Routing*: The extension line is routed dorsally through rigid 3D-printed guides and knotted to the top part of the triggering tip lever. The guides are glued to the dorsal side of the pocket and elevate the cable from the glove surface, preserving its alignment and ensuring a clear line of pull. The extension cable uncoils the shell back to its initial straight configuration and allows to control the transition speed during flexion.

C. Triggering Tip Lever

Triggering is achieved through a rigid 3D-printed lever, clamped to the distal tip of the longer multistable shell. Pulling either cable, the lever applies a torque on the distal end of the shell, triggering the transition between states in both directions (i.e., from straight to curled and vice versa). The geometry of the lever is iteratively optimized through force testing to minimize both the required triggering force and the overall bulk, ensuring effective actuation without compromising wearability.

D. Cable-Driven Actuation Module and Transmission

The actuation module, that drives Bowden cables for extension and flexion, is composed of a power transmission system, housed in a 3D-printed casing (Figure 3). The system is powered by a DC motor (DCX14L GB KL 6 V, ϕ14 mm, 10.5 W), equipped with a planetary gearhead (Maxon GPX16 A, 83:1) and a secondary spur gear reduction (50:18). The cables are wrapped around an array of spools with diameters of 23 mm, 20 mm, and 10.3 mm, intended for the actuation of thumb, index, and middle fingers. These dimensions are determined based on the first hand postural synergy [5]. The different spool diameters result in different cable velocities and force levels. In the present study only the index finger spool was employed; multi-finger effects will be investigated in future work. A feeder mechanism, utilizing one-way clutches and idle rollers, is integrated to introduce direction-dependent friction, preventing cable slackening or derailing during rapid snap-through events [15].

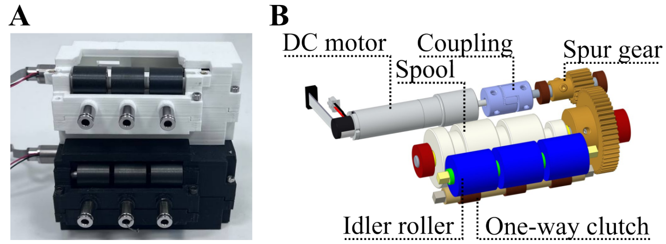

Fig. 3: (**A**) Picture of the two cable-driven actuation modules for flexion and extension. (**B**) Exploded view of the actuation module. The cables are wrapped around an array of three pairs of spools to actuate the thumb, index and middle finger. A feeder mechanism allows to avoid the slacking of the cable around the spool.

IV. EXPERIMENTAL EVALUATION

We investigated different designs of the triggering tip lever to identify the geometry that provides the best trade-off between activation force and distal bulk. Adopting the identified lever design, we then quantified the energy efficiency and dynamic performance of the resulting system. Energy efficiency was assessed by measuring electrical power consumption. Dynamic performance was characterized through bandwidth analysis and measurements of the minimum closure time during passive snap-through events.

A. Experimental Setup

The experimental setup shown in Figure 4A consists of an index mock-up finger, equipped with the actuation unit and mounted on a rigid frame. The index mock-up finger is a 3D-printed model designed based on the 50th male percentile [14]. Two cable-driven actuation modules control flexion and extension of the unit, respectively.

A passive linear guide enables the multistable shells to slide along the longitudinal axis of the finger during flexion, avoiding mechanical binding of the actuation system. Cables from the remote cable-driven actuation modules are fed through two spools to the actuation unit.

B. Cable Tension Required for Shell Activation

To evaluate the cable tension required to activate the multistable shells, a 6-axis load cell ((M3712A, SRI Sensor, China) was integrated into the cable path (Figure 4B). Before reaching the actuation unit, the cable was routed over a custom-designed spool mounted directly on the load cell. The spool incorporated a bearing wheel to significantly reduce friction between the cable and the sensing interface and to guide the cable such that the applied force was predominantly normal to the load cell surface. By exploiting the known geometry of the system, the cable tension was derived. After passing over the load cell, the cable was redirected to its

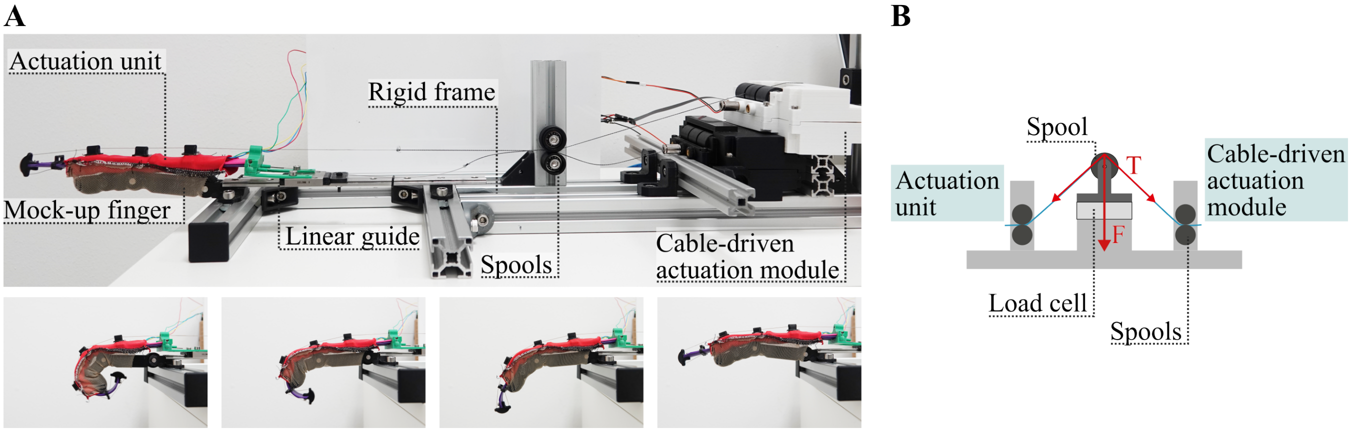

Fig. 4: (**A**) View of the experimental set-up. The mock-up finger is mounted on a rigid frame and equipped with the actuation unit, controlled by two cable-driven actuation modules. Representative snapshots of different flexion–extension phases are reported. (**B**) Schematics of the load cell integration in the cable path used to measure the force required for shell activation.

original trajectory toward the actuation unit.
The cable tension required to trigger shell activation was quantified for six (A-F) different designs of the triggering tip lever. For each design, force signals were sampled at 100 Hz during 10 flexion-extension (FE) cycles.

C. Power Consumption

Power consumption was quantified by recording electrical energy demand during flexion-extension cycles. Voltage and current were monitored using a current sensor (INA219) at 50 Hz. An integrated flex sensor (Bend Labs, Salt Lake City, UT, USA), placed into specific cavities on the actuation unit, monitored global finger curvature throughout the movement. For a comprehensive evaluation of the power consumption in each phase of the FE cycle, the test followed a specific multi-phase sequence:

1) The motor pulls the flexion cable to initiate snap-through. Snap-through is identified when the curvature reaches a critical predefined value;
2) Both cables are fed out to allow complete flexion;
3) The motors are deactivated for 2 s;
4) The extension cable is pulled until the measured curvature is zero, meaning that the multistable shells snapped in the straight state;
5) Extension cable is fed out by a predefined length;
6) The motors are deactivated for 2 s.

We evaluated the power consumption of the system over 20 complete FE cycles.

D. Actuation Bandwidth Characterization

To determine the bandwidth of the extension line in controlling the snap-through of the multistable shells, the motor was excited with a PWM signal with duty cycle s given by

$$s(t) = Asin(2pf(t)),$$
$$f(t) = f0 + \frac{(f1 - f0)t}{T},$$

that is, a linear up-chirp where $f_0 = 0.05\,\mathrm{Hz}$ is the initial frequency, $f_1 = 1\,\mathrm{Hz}$ is the final one, and $T = 30\,\mathrm{s}$ is the duration of the signal. The amplitude A was chosen so as to span a quarter range of a typical finger motion [5], avoiding state transitions of the multistable shells. The resulting angular displacement was monitored using an encoder on the cable-driven actuation module shaft (Maxon ENX10 EASY 1024IMP). Data acquisition was performed using an Arduino MKR Wifi 1010 board at a sampling frequency of 100 Hz. Bandwidth was defined as the $-3\,\mathrm{dB}$ attenuation frequency relative to low-frequency response.

E. Finger Motion Dynamic Response

The dynamic response of the actuated finger was evaluated by applying a triangular motor command with progressively increasing amplitude. The characterization was conducted within the operational bandwidth of the device. The input signal was provided as a PWM command to the motor driving the cable-based actuation system. Finger motion was measured using the flex sensor mounted on the dorsal side of the multistable shells. Flex sensor output was synchronized with motor encoder measurements. Both signals were synchronized and analyzed to quantify the relationship between motor actuation and finger flexion response. The system response was evaluated by comparing the commanded motor motion and the resulting finger kinematics, providing insight into the transmission characteristics and actuation effectiveness of the cable-driven multistable finger mechanism.

F. Minimum Closure Time

The minimum closure time was experimentally evaluated during 20 passive snap-through events. During flexion, the extension cable was fully released to eliminate motor constraints. The flexion motor triggered snap-through without imposing velocity limitations. Finger motion was therefore driven solely by the multistable shell dynamics. Closure time was defined as the interval between snap initiation and motion completion. Snap initiation was identified from a sudden change in flex sensor signal. Motion completion corresponded to stabilization in the fully flexed configuration. The measured closure time represents the intrinsic dynamic limit of the system.

V. RESULTS AND DISCUSSION

A. Cable Tension Required for Shell Activation

Median cable tensions across lever geometries varied between a maximum value of 7.53 N, for tip lever design F, and a minimum of 4.07 N, for design C, indicating a strong influence of tip design on activation efficiency (see Figure 5A). Lever designs C and E exhibited comparable median activation forces of 4.07 N and 4.13 N, although with different interquartile ranges (IQR), with design C showing lower variability (0.11 N compared to 0.17 N). The improved performance of design C and E can be attributed to their geometry, which increases the effective moment arm. In contrast to design E, the half-round profile of design C also enhances contact stability. This feature likely reduces localized slipping and improves force transmission consistency during activation. Based on these results, tip lever C was selected for subsequent experiments.

B. Power Consumption

The power consumption trend is shown in Figure 5B. During the flexion phase, the maximum median power absorbed by motors was 851 mW (IQR: 748 – 1050), occurring during the triggering of the snap-through condition at the tip of the actuator (1); after this event, the system passively reached the coiled state (2). During the extension phase (4), the median power required by the motor reached 1069 mW (IQR: 938 – 1160), corresponding to the energy input needed to fully re-extend the actuator. During the pauses after both flexion and extension phases (3),(6), power consumption rapidly dropped to approximately zero with median value of 4.00 mW (IQR = 1.67 mW). This evaluation validates the functional decoupling of active motor control from passive posture maintenance. Direct comparison with existing wearable hand exosuits is challenging, as power consumption during static posture maintenance is rarely reported under comparable conditions. While most cable-driven systems rely on continuous motor engagement, alternative non-backdrivable transmissions can also provide passive posture maintenance. However, these systems rely on low efficiency or require complex mechanisms [16]. Unlike these approaches, the proposed system maintains a simple design and additionally exploits stored elastic energy to generate rapid motions. Therefore, the near-zero motor power consumption observed during static posture holding suggests a qualitative difference rather than enabling a direct numerical comparison.

C. Actuation Bandwidth Characterization

Figure 6A shows the non-parametric Bode plot of the motor unit, obtained from input–output data using frequency-response estimation in the Fourier domain. The system presents a bandwidth of 0.49 Hz, which translates into a maximum cable retraction speed from a minimum of 0.024 m/s

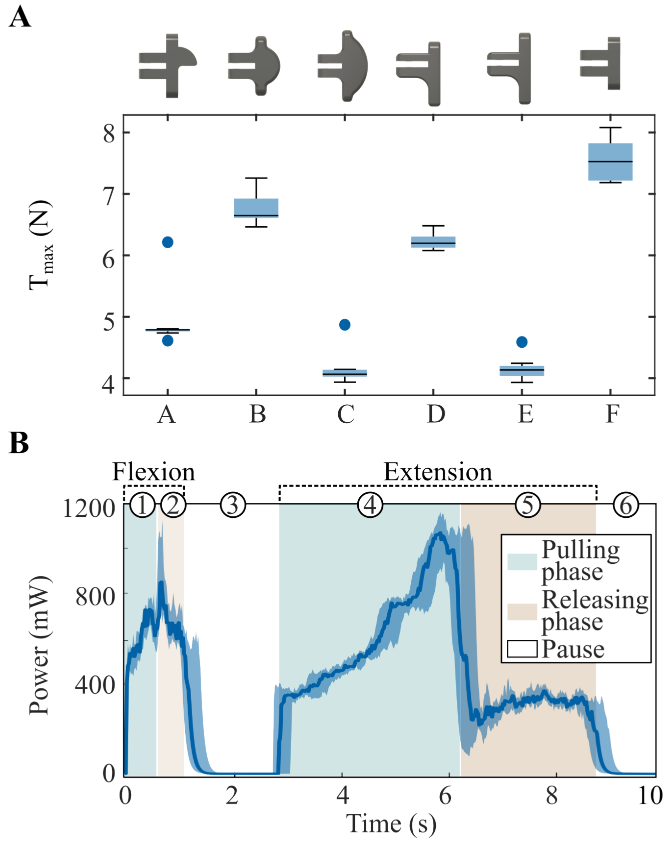

Fig. 5: (**A**) Design of six triggering tip lever with the cable tension required for shell activation, acquired with a load cell as schematize in Figure 4B. (**B**) System power consumption of the motors during a complete FE cycle. Phases 3 and 6 denote the straight configuration and the curled configuration, respectively.

(thumb spool) to a maximum of 0.054 m/s (middle finger spool). The measured system bandwidth remains limited compared to values reported in the literature [5], reflecting the constraints imposed by cable-driven transmission and motor dynamics. In contrast, the snap-through behavior of the multistable shells enables fast state transitions that are not governed by the measured bandwidth. Therefore, bandwidth characterization is used here to define the possibility to control the system in flexion after snap-through, rather than the speed of the transition itself.

D. Finger Motion Dynamic Response

The system response was quantified in terms of amplitude attenuation and temporal delay between the motor command and the resulting finger motion. The experimental data show attenuation and delay between motor motion and finger response, which can be observed in Figure 6B. The amplitude ratio ranged between approximately 24% and 54%, while the measured delay ranged between 0.26 s and 2.75 s depending on the excitation condition. This behavior reflects the combined effects of cable compliance, friction losses, and mechanical dynamics of the multistable structure. Overall, the results indicate that the cable-driven actuation system

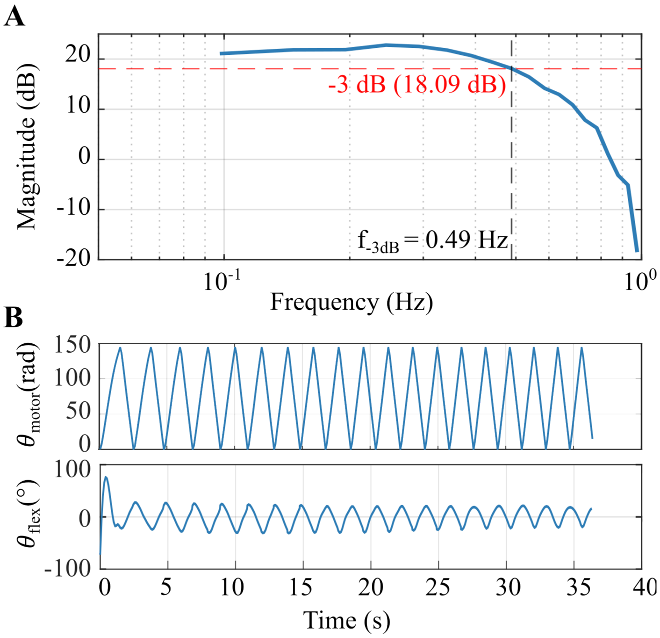

Fig. 6: (**A**) Magnitude of the Bode plot for the transfer between the resulting shaft rotation and the motor input. The system exhibits an actuation bandwidth of 0.49 Hz, identified at the -3 dB attenuation frequency. (**B**) Motor angular position reconstructed from encoder counts and flexion sensor signal filtered and centered around zero.

introduces both amplitude reduction and latency between the motor input and finger output, which become more pronounced under faster or larger actuation commands.

E. Minimum Closure Time

Finger closure occurred within 0.53 ± 0.13 s, measured from snap initiation to stabilization. Closure time was consistent across trials, suggesting repeatable passive dynamics despite moderate inter-trial variability. Closure time showed no dependence on motor command amplitude or actuation speed. This confirms that closure dynamics are governed by the multistable shell behavior. The measured value defines a lower bound on achievable finger actuation speed. In the proposed architecture, closure speed exceeds the bandwidth-limited response of the cable transmission and is primarily determined by shell snap-through dynamics. These results highlight the potential of multistable elements to enable rapid finger closure once the snap-through transition has been triggered, regardless the limitations introduced by the specific actuation and transmission systems employed.

VI. CONCLUSION

In this work we proposed and experimentally characterized a cable-driven actuation unit that integrates multistable elastic shells. Experimental results confirmed that posture holding can be achieved with near-zero motor power consumption, while finger closure speed during snap-through events is governed primarily by the intrinsic dynamics of the multistable shells rather than by motor velocity. These findings support our initial hypothesis that multistable elements can be used to functionally decouple static posture maintenance from active motor control in wearable hand devices, significantly increasing battery life. Future work will focus on extending the proposed actuation concept to a fully integrated multi-finger glove, implementing fingers synergies, as well as an agonistic–antagonistic strategy with flexion and extension both driven by a single motor. Finally, long-term durability testing of the multistable shells under repeated cycling, together with user-in-the-loop experiments to evaluate functional performance during grasping tasks, will enable a comprehensive assessment of the proposed approach in realistic operating scenarios.

REFERENCES

[1] R. S. Mosher, "Handyman to hardiman," *Sae Transactions*, pp. 588–597, 1968.

[2] A. Manero, V. Rivera, Q. Fu, J. D. Schwartzman, H. Prock-Gibbs, N. Shah, D. Gandhi, E. White, K. E. Crawford, and M. J. Coathup, "Emerging medical technologies and their use in bionic repair and human augmentation," *Bioengineering*, vol. 11, no. 7, p. 695, 2024.

[3] J. Mehrholz, M. Pohl, T. Platz, J. Kugler, and B. Elsner, "Electromechanical and robot-assisted arm training for improving activities of daily living, arm function, and arm muscle strength after stroke," *Cochrane database of systematic reviews*, no. 9, 2018.

[4] T. Bagneschi, D. Chiaradia, G. Righi, G. Del Popolo, A. Frisoli, and D. Leonardis, "A soft hand exoskeleton with a novel tendon layout to improve stable wearing in grasping assistance," *IEEE Transactions on Haptics*, vol. 16, no. 2, pp. 311–321, 2023.

[5] M. Xiloyannis, L. Cappello, D. B. Khanh, S.-C. Yen, and L. Masia, "Modelling and design of a synergy-based actuator for a tendon-driven soft robotic glove," in *2016 6th IEEE international conference on biomedical robotics and biomechatronics (BioRob)*. IEEE, pp. 1213–1219.

[6] R. Alicea, M. Xiloyannis, D. Chiaradia, M. Barsotti, A. Frisoli, and L. Masia, "A soft, synergy-based robotic glove for grasping assistance," vol. 2, p. e4, ISBN: 2631-7176.

[7] T. Du Plessis, K. Djouani, and C. Oosthuizen, "A review of active hand exoskeletons for rehabilitation and assistance," vol. 10, no. 1, p. 40, ISBN: 2218-6581.

[8] S. D. Guest and S. Pellegrino, "Analytical models for bistable cylindrical shells," vol. 462, no. 2067, pp. 839–854, ISBN: 1364-5021.

[9] Y. Chi, Y. Li, Y. Zhao, Y. Hong, Y. Tang, and J. Yin, "Bistable and multistable actuators for soft robots: Structures, materials, and functionalities," vol. 34, no. 19, p. 2110384, ISBN: 0935-9648.

[10] Y. Lin, D. Zhu, A. Naidu, K. Yu, D. Harper, E. Halilaj, D. Weber, D. Kenney, A. J. Popchak, M. Baratz *et al.*, "Personalized bistable orthoses for rehabilitation of finger joints," in *Proceedings of the 38th Annual ACM Symposium on User Interface Software and Technology*, 2025, pp. 1–18.

[11] E. Kebadze, S. Guest, and S. Pellegrino, "Bistable prestressed shell structures," *International Journal of Solids and Structures*, vol. 41, no. 11-12, pp. 2801–2820, 2004.

[12] K. Iqbal and S. Pellegrino, "Bi-stable composite shells," in *41st structures, structural dynamics, and materials conference and exhibit*, 2000, p. 1385.

[13] R. M. Jones, *Mechanics of composite materials*. CRC press, 2018.

[14] T. M. Greiner, "Hand anthropometry of us army personnel," Tech. Rep., 1991.

[15] H. In, B. B. Kang, M. Sin, and K.-J. Cho, "Exo-glove: A wearable robot for the hand with a soft tendon routing system," *IEEE Robotics & Automation Magazine*, vol. 22, no. 1, pp. 97–105, 2015.

[16] M. Controzzi, L. B. Luciani, and F. Montagnani, "Unified approach to bi-directional non-back drivable roller clutch design," *Mechanism and Machine Theory*, vol. 116, pp. 433–450, 2017.